

# Asymmetric feed circularly polarized broadband printed antenna for wireless communication

MD. TARIKUL ISLAM<sup>a,\*</sup>, MD. SAMSUZZAMAN<sup>a,b</sup>, M. N. RAHMAN<sup>b</sup>, MANDEEP JIT SINGH<sup>a</sup>,  
MOHAMMAD TARIQUL ISLAM<sup>a</sup>

<sup>a</sup>*Department of Electrical, Electronic and Systems Engineering, Faculty of Engineering and Built Environment  
Universiti Kebangsaan Malaysia, Bangi, Selangor, 43600, Malaysia*

<sup>b</sup>*Patuakhali Science and Technology University, Dumki, 8602, Bangladesh*

In this paper, the design of a new wideband circularly polarized (CP) patch antenna is presented. The design principle of this antenna is different from the conventional monopole antennas. The antenna complies with an asymmetric microstrip-line feed modified etched rectangular radiator printed on top of a substrate. Another radiator is printed on the bottom of the substrate which acts as a ground plane. The antenna covers a total electrical dimension of  $0.180\lambda \times 0.318\lambda \times 0.005\lambda$  at the first resonant frequency of 900 MHz. Both the radiators are asymmetrically configured that results in the surface current becomes orthogonal and creates circular polarization. The initial design is simulated in HFSS and after fabrication, the performance is compared with the simulated results. The prototype covers an impedance bandwidth of 118% (900 MHz to 3.6 GHz) under 10dB return loss and axial ratio bandwidth of 101% (1.84 GHz to 5.4 GHz). With the maximum gain of 5.6 dBi, the antenna has a constant growing gain with circular polarization. A detailed parametric study on design and current distribution is carried out to validate the antennas CP mechanism.

(Received November 17, 2018; accepted April 9, 2020)

**Keywords:** Asymmetric feed, Axial ratio, Broadband, Circular polarization, Printed antenna

## 1. Introduction

The petition for improved antenna performance has increased with the development of wireless communication systems. CP antennas are a good candidate for the use of sensor systems and many more communication systems for its high resistance to Faraday effect and enhanced polarization matching with respect to multipath propagation [1-3]. The main use of circular polarization is satellite locating, satellite communication link, radio frequency identification (RFID) systems for its intrinsic benefit depolarization effect of insensitivity and to optimize the performance of sensor system [4-8]. The circular polarization can be generated if two degenerated phases with an angle of  $90^\circ$  are both excited simultaneously. It is noticed that for mode 2 the frequency response is agitated hence the mode 2 amplitude is similar to mode 1 and located at  $90^\circ$  face difference at the operating frequency.

In literature, several types of circularly polarized antenna have been reported [9-21]. The microstrip patch disrupts by a narrow slot that creates circular polarization [9, 22]. A wideband antenna has the ability to switch its polarization with the E-shaped radiating patch was proposed in [10], but these devices are complex assembly and high manufacturing cost. There are several antennas proposed for the enhancement of the bandwidth such as circular with parasitic loop [11], dual rectangular wire loop [13] and dual-layer substrate [14], that achieved the axial ration bandwidth of 16%, 18%, and 9.6%, respectively. By adopting a cross-coupler, the polarization diversity was realized [12, 15, 16, 18]. A co-designed

filtering annular slot antenna was reported in [17]. Multi-layer dimensions are complex and not appropriate for the low-profile application. Slotted Low profile, hook shaped [23], cross shaped [24] antennas with CP characteristics were reported in [25, 26]. In [27], a broadband CP antenna was reported where the patch was connected to the transmission line by four different sized slots. The high rate of data transmission is not possible in a wireless system with a narrow 3-dB axial ratio (AR). To overcome this problem and to enhance the CP bandwidth, slot antennas are tested for its low profile, wider bandwidth, and easy fabrication. The AR bandwidth has increased more than 19% in [28] by applying a square slot along with the junction and T-shaped band. In addition, for achieving 56.5% of CP bandwidth a falcate-shaped slot and two specific feed lines were proposed in [29]. Nevertheless, the axial ratio was not bounded by operating bandwidth. A dipole antenna having two feeding lines in a face difference of  $90^\circ$  was proposed in [30, 31] to enhance the AR and impedance bandwidth. The attempt to achieve CP in [32], an artificial ground is attached with a dipole. In [33], a dual T-shaped feed line was stripped with the ground by asymmetric lines to achieve CP bandwidth. While the AR bandwidth of the reported antennas in [29, 34] and [33] have increased but the antenna size is large. By introducing the asymmetric feed line, the impedance bandwidth of a planar antenna with the small ground can be improved [35]. Also, unidirectional radiation patterns can be generated by asymmetric feeding [36]. There is a significant effect of the ground plane for achieving broadband operation. Planar dipoles can be redefined from different printed monopole configurations and stated in

[37]. The coupling capacitance can be reproduced by balancing the gap between the patch and ground plane [38]. A L-shaped antenna with two asymmetric microstrip-fed line was proposed for achieving RHCP and LHCP [39]. There is still a challenge to design a compact broadband CP antenna with wider AR bandwidth.

As per the author's concern, very few tries have been carried out so far for generating CP by trepidation of traditional dipole/monopole antennas. In this paper, a new feeding technique of the asymmetric line is connected to a patch that acts as the main radiating element and stands against the ground plane at  $90^\circ$  phase angle to generate circular polarization. Supplementary, the ground plane also at the asymmetric radiating element. Four truncate cuts at two edges of both patch and ground help to achieve wider bandwidth.

## 2. Antenna design and analysis

### 2.1. Antenna geometric layout

The geometry of the proposed CP antennas top and a cross-sectional view is shown in Fig. 1. The antenna structure is diverted from the conventional symmetric feed monopole antenna. The prototype is configured with two modified rectangular radiating elements etched at the corner and printed on RT/Duroid substrate with 2.2 dielectric constant and 1.57mm of thickness. The substrate is used for its low loss dielectric constant. One of them is acts as a patch and another one-act like the ground and fed by a  $50\Omega$  asymmetric transmission line. The patch and ground are designed in a plane so that they are at  $90^\circ$  phase difference. The patch is excited towards the +X direction by the fed line and the ground is excited at -X direction and both are separated by the gap distance of "g" along with Y direction. The antenna covers the total dimension of  $106 \times 60 \times 1.57 \text{ mm}^3$ .

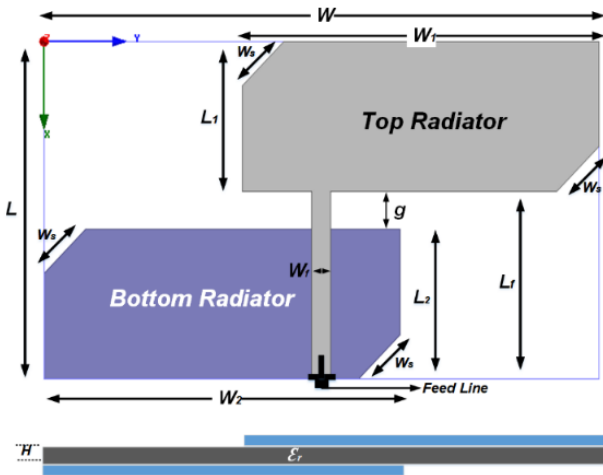


Fig. 1. Design geometry of the antenna top and cross-sectional view (color online)

### 2.2. Circular polarization principle

The conventional monopole antennas are more or less horizontally or vertically polarized where one direction is stronger than the other one. So, it is difficult to achieve circular polarization from these types of antennas. The circular polarization can be achieved with a similar amplitude and phase alteration of  $90^\circ$  along with dual E-vectors at orthogonal planes. Two orthogonal currents including horizontal and vertical have been produced by configuring the asymmetric feeding technique across the radiating elements. This caused the dual orthogonal vectors including  $E_{Ver}$  and  $E_{Hor}$ . The principle of generating circular polarization can be described with the current distribution of both the radiator. Basically, this modified dimension of the antenna is chosen for attaining longitudinal currents. The X-directed current produces E-field ( $E_{Hor}$ ) and similarly the Y-directed current bring E-field ( $E_{Ver}$ ). The ideal distance of the radiators gives  $90^\circ$  phase angle. The primary design parameters are length  $L$ , width  $W$ , feed line  $L_f$ , etched corner  $W_s$ , gap 'g' between patch and ground. To achieve maximum RHCP performance the design parameters are attuned and the axial ratio bandwidth is achieved below 3dB. The AR bandwidth is achieved above 5GHz for choosing a suitable size of the stub. The modified design parameters are enumerated in Table 1.

Table 1. Different adjusted parameters

Label	Dimension (mm)	Label	Dimension (mm)
$L$	106	$L_f$	33.8
$W$	60	$G$	6.8
$W_1, W_2$	68	$W_f$	3.6
$L_1, L_2$	27	$W_s$	11.31
$H$	1.57		

### 2.3. Surface current distribution

The prototype is designed for achieving left-hand circular polarization (LHCP) towards the +Z direction. Fig. 2 shows the surface current distribution for the orientation of  $0^\circ$  to  $270^\circ$  at the resonant frequency of 2.1 GHz. The surface current is focused on the -X direction for  $0^\circ$  phase. The dominating current flows to +Y direction at  $90^\circ$  phase. For  $180^\circ$ , most of the current is directed to +X direction. Lastly, the current flows through -Y direction at  $270^\circ$  phase and polarization is towards +Z direction. From this observation, it is clear that the antenna can generate LHCP polarization. From this configuration, right-hand CP also can be achieved by swapping the position of the top and bottom radiator.

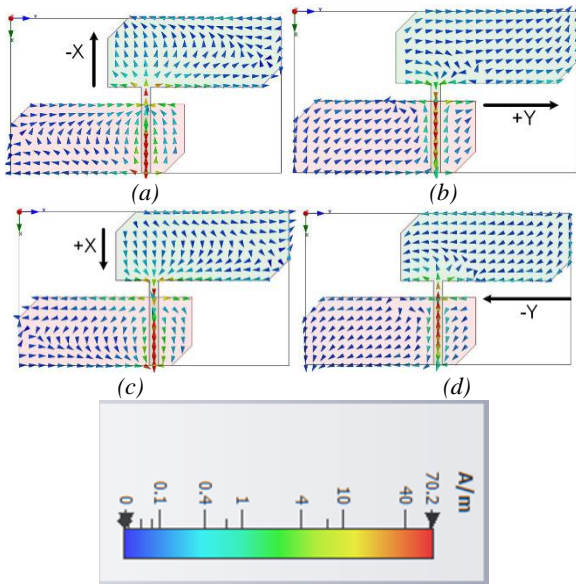


Fig. 2. Surface current distribution at (a)  $0^\circ$  (b)  $90^\circ$  (c)  $180^\circ$  and (d)  $270^\circ$  (color online)

### 3. Parametric study

The consequence of different modifications of the antenna design on impedance bandwidth and AR bandwidth is stated in this segment. The type of substrate material and dimension of the resonators has a significant effect on bandwidth and antenna gain. A parametric study is necessary for suitable dimension selection to achieve the desired antenna specification. Figs. 3 and 4 represent the simulated reflection coefficient and AR with respect to frequency. Different measurement of the length of the radiators  $W_1$  and  $W_2$  have an effect on both the properties. In Fig. 3 it is clear that  $W_1$  and  $W_2$  have a minimal effect on impedance bandwidth even its length is increasing. Furthermore, the same effect on AR bandwidth. No significant change with respect to the change of length of the radiators. However, the mid-value of the width parametric reaches the maximum desirable results. The outcome of top and bottom radiator width  $L_1$  and  $L_2$  over the impedance and AR bandwidth is shown in Figs. 5 and 6. The parameter has a major effect on both impedance and AR bandwidth. From Fig. 5 it is clear that by decreasing and increasing the width of resonators the wideband performance reduces remarkably. Fig. 6 shows that the increasing  $L_1$  and  $L_2$  values lost the AR limit beyond 3dB. The proposed length has a significant improvement in the CP and AR bandwidth.

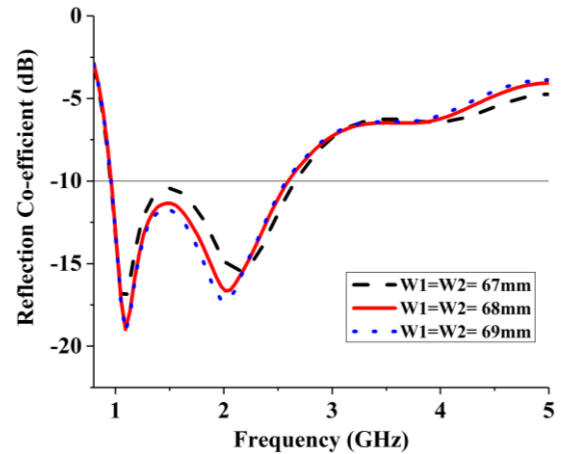


Fig. 3. Evaluation of the  $S_{11}$  for different width of resonators (color online)

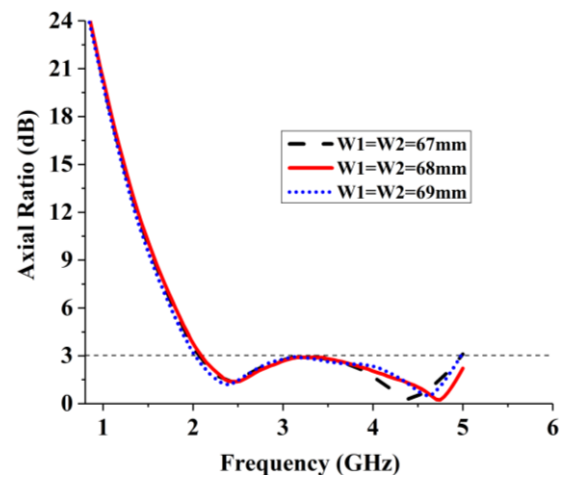


Fig. 4. Evaluation of axial ratio (AR) for different width of resonators (color online)

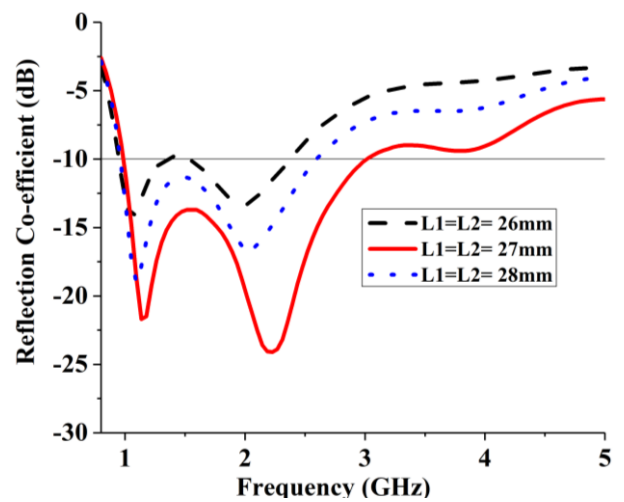


Fig. 5. Evaluation of the  $S_{11}$  for different length of resonators (color online)

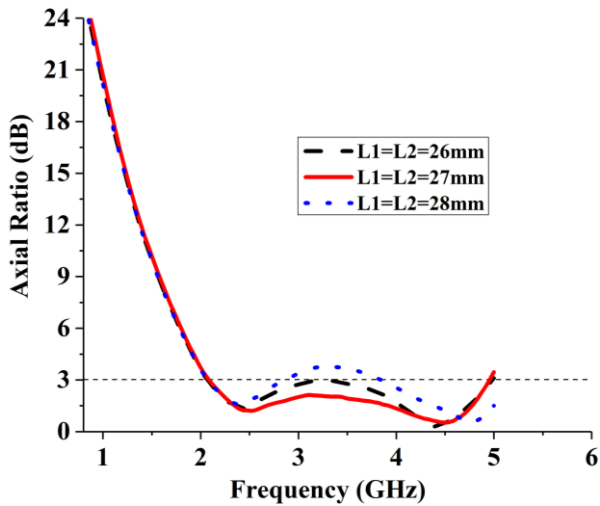


Fig. 6. Evaluation of axial ratio (AR) for different length of resonators (color online)

#### 4. Experimental results and discussions

The proposed antenna performance is analyzed by the HFSS simulation solver which acts on the basis of the Finite Element Method. The fabricated prototype is shown in Fig. 7 and the performance is measured and compared with the simulated results. A PNA series Network analyzer was used for the measurement of the reflection coefficient ( $S_{11}$ ) of the fabricated prototype. StarLab near-field antenna measurement system as shown in Fig. 8 is used to measure the radiation pattern, axial ratio and gain of the prototype. The system has the facility to measure the electric fields of the antenna in the near field region for computing the equivalent far-field values of the antenna under test (AUT). The AUT is positioned in the middle of a circular “arch” and placed on the testbed which consists of 16 separate receiving antennas. The antennas are placed circularly with maintaining the same distance. The AUT is rotated  $360^\circ$  horizontally and this turning and array antennas make a full 3D scan from which we get 3D radiation pattern. The gain and efficiency are computed from the far-field data.

The  $S_{11}$  results of the modified design is shown in figure 9. It is observed from the graph that the antenna achieves the fractional bandwidth of 118% (900 MHz to 3.5 GHz) under 10dB return loss. Due to fabrication error and cable loss, there is slight mismatch between the simulated and measurement result is observed. The overall design offers a wideband performance.



(a)



(b)

Fig. 7. Fabricated antenna prototype a) Top view b) Bottom view (color online)

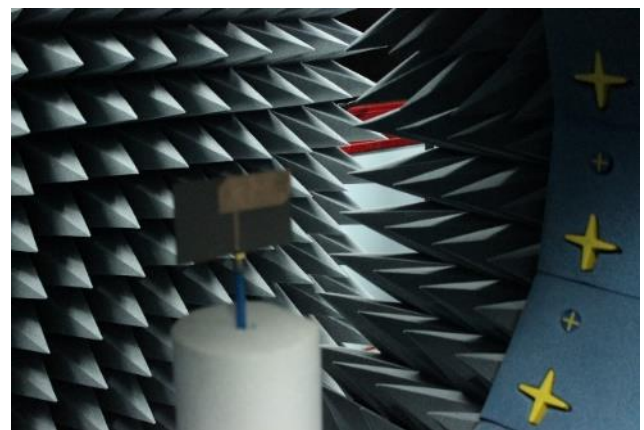


Fig. 8. Satimo Star Lab measurement in UKM (color online)

The simulated and measured Axial ratio bandwidth of the antenna at the 3-dB is shown in Fig. 10. The results show that the antenna has the 3dB axial ratio bandwidth of 101% (1.7-5.2 GHz). Fig. 11 shows the simulated and experimental peak realized gain over the CP band. The maximum gain is recorded as 5.6dBi at 3.2 GHz. Also, the antenna shows good gain over the CP band.

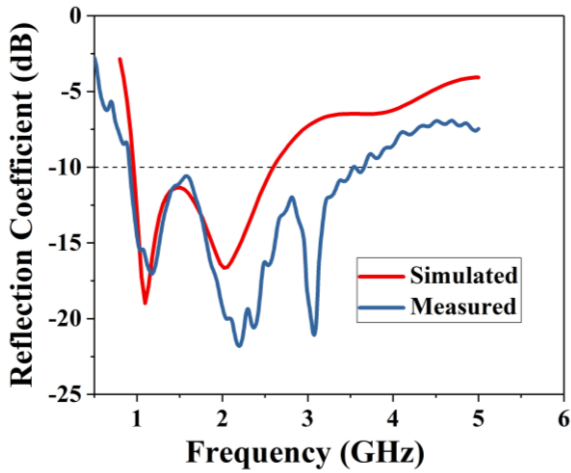


Fig. 9. Simulated and Measured Reflection Co-efficient of the proposed prototype (color online)

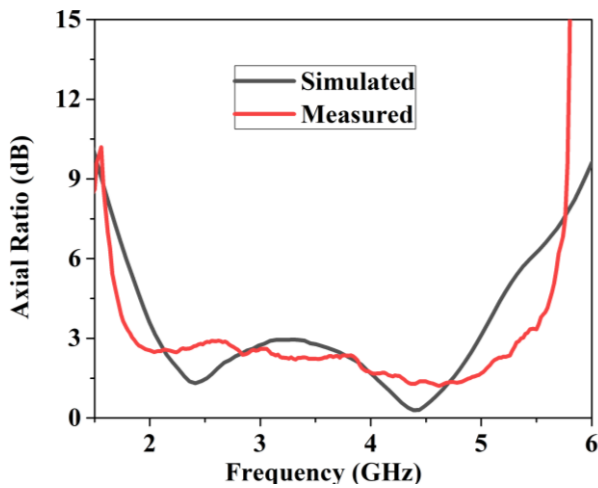


Fig. 10. Simulated and measured axial ratio bandwidth (color online)

Fig. 12(a) displays the measured 2D linear polarized radiation patterns of the co-polarized field and cross-polarized field in the two principles plane-namely E-(XZ) and H (YZ)-plane at 1.2 GHz frequencies. From the figure, it can be stated that at low frequencies, the co-polarization field is omnidirectional and the cross-polarization field is slightly directional in both E- and H planes. As the frequency increases, higher-order current modes are excited, and the radiation patterns become more directional, with slight deformations.

On the other hand, Fig. 12(b) shows the measured 2D circular polarized radiation patterns of the LHCP (Left Hand Circular polarized) field and RHCP (Right Hand Circular Polarized) field in the two principles plane-namely E-(XZ) and H (YZ)-plane at 2.1 GHz frequencies. It can be comprehended from this figure that the proposed antenna attains good performance of left-hand circularly polarized (LHCP) radiation in the  $+z$ -direction and right hand circularly polarized (RHCP) radiation in the  $-z$ -direction.

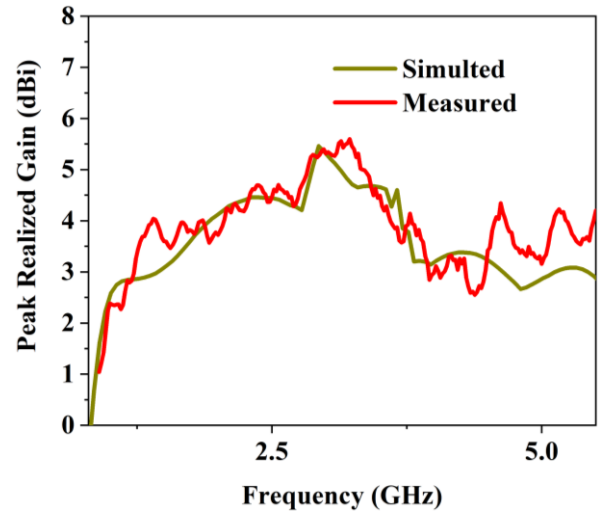


Fig. 11. Simulated and measured gain against frequency (color online)

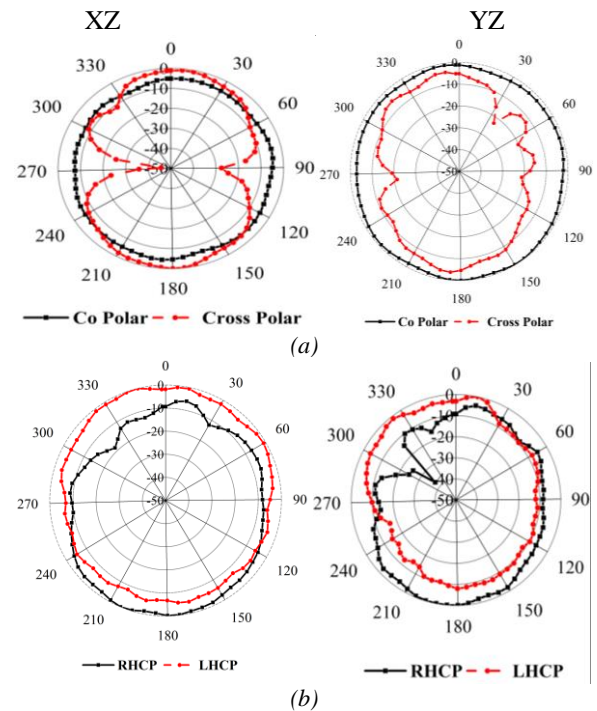


Fig. 12. Radiation pattern at (a) 1.2 GHz (Linear Polarization); (b) 2.1 GHz (Circular polarization) (color online)

A detailed comparison of the specification of the proposed and similar recently reported antennas are listed in Table 2. It is investigated that the proposed antenna has higher fraction bandwidth for both impedance and AR, and compact simple design structure.

Table 2. Performance comparison of different CP antennas

References	Size(mm <sup>3</sup> )	CP center frequency (GHz)	-10 dB Bandwidth	3-dB AR bandwidth	Radiation pattern
[1]	100×70×1.5	1.8	78.7%	27.5%	Unidirectional
[4]	100×200×23	2.5	30%	10%	Unidirectional
[10]	140×80×0.5	2.4	7%	13%	Unidirectional
[13]	157×52×10	1.5	22%	18%	Bidirectional
[15]	252×252×20	0.89	28.6%	18%	Unidirectional
[28]	120×65×1	2.65	40%	20.76%	Bidirectional
[29]	50×50×0.76	6.4	31	56.47%	Bidirectional
Proposed	106×60×1.57	2.3	118%	101%	Bidirectional

## 5. Conclusion

A broadband CP antenna with new asymmetric feed line technology has been presented. The antenna constructed with two resonators connected to an asymmetric fed line of 50Ω. The antenna can operate under 3dB AR band from 1.7-5.2 GHz and 10dB return loss from 900 MHz to 3.5 GHz. The fractional bandwidth of impedance and AR is 118% and 101%, respectively. A detailed parametric study is carried out to validate and get the optimum dimension for the desired specification. The surface current distribution also observed to understand the circular polarization. 2D and 3D RHCP and LHCP radiation patterns also described. With the stable gain, the antenna can be a suitable candidate for various wireless communication applications such as global positioning, sensor and various vehicular application for its simplicity and compactness.

## Acknowledgments

This work is supported by Universiti Kebangsaan Malaysia research grant GUP-2019-074.

## References

- [1] W. Cao, B. Zhang, T. Yu, H. Li, IEEE Antennas and Wireless Propagation Letters **9**, 1065 (2010).
- [2] K. Ding, C. Gao, T. Yu, D. Qu, IEEE Transactions on Antennas and Propagation **63**(2), 785 (2015).
- [3] Q. Liu, Z. N. Chen, Y. Liu, C. Li, IEEE Transactions on Antennas and Propagation **65**(4), 2129 (2017).
- [4] F.-S. Chang, K.-L. Wong, T.-W. Chiou, IEEE Transactions on Antennas and Propagation **51**(10), 3006 (2003).
- [5] F. Ferrero, C. Luxey, G. Jacquemod, R. Staraj, IEEE Antennas and Wireless Propagation Letters **4**(1), 13 (2005).
- [6] H. W. Kwa, X. Qing, Z. N. Chen, Antennas and Propagation Society International Symposium, 2008. AP-S 2008. IEEE, 2008: IEEE, p. 1.
- [7] R. Azim et al., 2015 International Conference on Space Science and Communication (IconSpace), 2015: IEEE, p. 402.
- [8] M. Samsuzzaman, M. T. Islam, M. Nahar, J. Mandeep, F. Mansor, M. Islam, International Journal of Applied Electromagnetics and Mechanics **47**(4), 1039 (2015).
- [9] X. Bao, M. Ammann, Journal of Electromagnetic Waves and Applications **20**(11), 1427 (2006).
- [10] A. Khidre, K.-F. Lee, F. Yang, A. Z. Elsherbeni, IEEE Transactions on Antennas and Propagation **61**(2), 960 (2013).
- [11] R. Li, J. Laskar, M. Tentzeris, Electronics Letters **41**(18), 997 (2005).
- [12] V. Rafiei, H. Saygin, S. Karamzadeh, Applied Computational Electromagnetics Society Journal **32**(12), 1117 (2017).
- [13] M. Sumi, K. Hirasawa, S. Shi, IEEE Transactions on Antennas and Propagation **52**(2), 551 (2004).
- [14] S. Gao, Y. Qin, A. Sambell, IEEE Antennas and Propagation Magazine **49**(4), 57 (2007).
- [15] X.-Z. Lai, Z.-M. Xie, Q.-Q. Xie, X.-L. Cen, IEEE Antennas and Wireless Propagation Letters **12**, 1630 (2013).
- [16] R. Ferreira, J. Joubert, J. W. Odendaal, IEEE Transactions on Antennas and Propagation **65**(1), 364 (2017).
- [17] J. Li, X. Zhang, J. Chen, J. Chen, K. Da Xu, A. Zhang, AEU-International Journal of Electronics and Communications **90**, 30 (2018).
- [18] S. Karamzadeh, V. Rafiei, H. Saygin, The Applied Computational Electromagnetics Society **32**(9), 789 (2017).
- [19] S. Ghosal, R. M. Shubair, arXiv preprint arXiv:1909.12988, 2019.
- [20] C. S. Lee, F. Yang, U.S. Patent 10,418,706, issued September 17, 2019.
- [21] Harine G, Pavone SC, Di Donato L, Di Mariano P, Distefano G, Livreri P, Prabagarane N, Squadrito C, Sorbello G, IEEE Antennas and Wireless Propagation Letters, 2020.
- [22] M. Samsuzzaman, M. T. Islam, M. J. Singh, IEEE Access **6**, 54713 (2018).
- [23] M. Samsuzzaman, M. T. Islam, Electronics Letters **50**(15), 1043 (2014).
- [24] M. Samsuzzaman, M. T. Islam, Microwave and Optical Technology Letters **56**(11), 2711 (2014).
- [25] S. Shi, K. Hirasawa, Z. N. Chen, IEEE Transactions on Antennas and Propagation **49**(11), 1517 (2001).
- [26] J.-S. Row, IEEE Transactions on Antennas and Propagation **53**(6), 1967 (2005).
- [27] C. Zhang, X. Liang, X. Bai, J. Geng, R. Jin, IEEE Antennas and Wireless Propagation Letters **13**, 1457 (2014).
- [28] G. Zhao, L. N. Chen, Y. C. Jiao, Microwave and Optical Technology Letters **50**(10), 2639 (2008).
- [29] S. Lee et al., Microwave and Optical Technology Letters **58**(9), 2245 (2016).
- [30] A. S. Andrenko, Antennas and Propagation, 2006. EuCAP 2006. First European Conference on, 2006: IEEE, p. 1.

- [31] J.-W. Baik, K.-J. Lee, W.-S. Yoon, T.-H. Lee, Y.-S. Kim, *Electronics Letters* **44**(13), 785 (2008).
- [32] F. Yang, Y. Rahmat-Samii, *IEEE Transactions on Antennas and Propagation* **53**(9), 3083 (2005).
- [33] R. K. Saini, S. Dwari, *IEEE Transactions on Antennas and Propagation* **64**(1), 290 (2016).
- [34] M. Samsuzzaman, M. T. Islam, S. Kibria, M. Cho, *Microwave and Optical Technology Letters* **57**(6), 1503 (2015).
- [35] M. John, J. Evans, M. Ammann, J. Modro, Z. Chen, *IET microwaves, antennas & propagation* **2**(1), 42 (2008).
- [36] K. Thomas, M. Sreenivasan, *IET microwaves, antennas & propagation* **5**(7), 831 (2011).
- [37] K. G. Thomas, M. Sreenivasan, *IEEE Transactions on Antennas and Propagation* **58**(1), 27 (2010).
- [38] A. M. Abbosh, M. E. Bialkowski, *IEEE Transactions on Antennas and Propagation* **56**(1), 17 (2008).
- [39] C. Wei, M. Zhou, K. Ding, F. X. Yu, J. J. Mo, X. L. Zhao, *Microwave and Optical Technology Letters* **60**(7), 1685 (2018).

---

\*Corresponding author: p94299@siswa.ukm.edu.my